



TeV Scale Singlet Dark Matter

Citation

Pontón, Eduardo, and Lisa Randall. 2009. TeV scale singlet dark matter. *Journal of High Energy Physics* 2009(4): 80.

Published Version

doi:10.1088/1126-6708/2009/04/080

Permanent link

<http://nrs.harvard.edu/urn-3:HUL.InstRepos:8052091>

Terms of Use

This article was downloaded from Harvard University's DASH repository, and is made available under the terms and conditions applicable to Open Access Policy Articles, as set forth at <http://nrs.harvard.edu/urn-3:HUL.InstRepos:dash.current.terms-of-use#OAP>

Share Your Story

The Harvard community has made this article openly available.
Please share how this access benefits you. [Submit a story](#).

[Accessibility](#)

TeV Scale Singlet Dark Matter

Eduardo Pontón^a and Lisa Randall^b,

*^aDepartment of Physics, Columbia University,
538 W. 120th St, New York, NY 10027, USA*

*^bJefferson Laboratory of Physics, Harvard University,
Cambridge, Massachusetts 02138, USA*

Abstract

It is well known that stable weak scale particles are viable dark matter candidates since the annihilation cross section is naturally about the right magnitude to leave the correct thermal residual abundance. Many dark matter searches have focused on relatively light dark matter consistent with weak couplings to the Standard Model. However, in a strongly coupled theory, or even if the coupling is just a few times bigger than the Standard Model couplings, dark matter can have TeV-scale mass with the correct thermal relic abundance. Here we consider neutral TeV-mass scalar dark matter, its necessary interactions, and potential signals. We consider signals both with and without higher-dimension operators generated by strong coupling at the TeV scale, as might happen for example in an RS scenario. We find some potential for detection in high energy photons that depends on the dark matter distribution. Detection in positrons at lower energies, such as those PAMELA probes, would be difficult though a higher energy positron signal could in principle be detectable over background. However, a light dark matter particle with higher-dimensional interactions consistent with a TeV cutoff can in principle match PAMELA data.

1 Introduction

Dark matter has received a lot of attention of late as new dark matter searches ramp up. Of particular interest is the increasing capacity to detect dark matter in both direct and indirect channels. The latter rely solely on dark matter annihilation, which is nice in that it doesn't assume any particular type of interaction with the Standard Model and furthermore the annihilation rate is generally connected to the annihilation cross section responsible for the current dark matter abundance.

Given the importance of dark matter searches and our lack of knowledge as to the true nature of dark matter, it makes sense to explore the range of possibilities and what their implications would be for current and future detectors. In this paper we will consider singlet dark matter candidates with mass of order one to a few TeV. We assume a Z_2 symmetry that prevents any operator allowing decay and therefore ensuring stability. This is perhaps the simplest dark matter candidate there can be. In fact, such a possibility has been previously considered in Ref. [1, 2, 3, 4], but in a lower mass region. In this paper we concentrate on the remaining allowed mass range, of order one to a few TeV, which phenomenologically is also a viable possibility. We concentrate on some novel scenarios that arise in a framework with a low cutoff scale.

Although we mostly take an agnostic approach about the source of this dark matter, we also focus on TeV scale particles that arise in a theory with a TeV cut-off scale. Such a scenario can occur for example in the RS framework [5]. See also [6] for a study of heavy DM in a supersymmetric theory with a relatively low cutoff.

In this paper we show the range of allowed parameters giving the right relic density and then consider whether such dark matter has any chance of being detected. We find that annihilation into photons might provide a visible signal at high energy gamma ray detectors such as HESS or VERITAS, particularly if higher-dimension operators are present. We also consider more model-dependent scenarios in which annihilation into positrons can also occur. We show the signal can exceed background with reasonable assumptions, but most likely not in the PAMELA range for a TeV-scale mass.

On the other hand, we observe that a dark matter candidate of about 100 GeV whose dominant decay mode involves direct positron emission, such as can occur with a higher-dimension operator suppressed by the TeV scale, matches PAMELA data quite nicely.

2 Singlet Dark Matter

We start by discussing the relic density computation for a thermally produced Standard Model singlet. We consider first a renormalizable four-dimensional theory. This analysis would of course also apply to a nonrenormalizable theory so long as the renormalizable coupling of the singlet scalar to a Higgs dominates annihilation, including a five-dimensional theory with a brane-bound scalar or any five-dimensional theory where the higher-dimension operators are suppressed.

We then consider a more exotic possibility that could in principle give rise to a detectable positron signal. We will see this scenario is unlikely to explain the PAMELA data, although it could give rise to a detectable signal in the high-energy positron range.

2.1 Thermal Relic Abundance for a Singlet

We assume a singlet field Φ protected by a discrete Z_2 symmetry $\Phi \rightarrow -\Phi$ in a nonrenormalizable theory with a TeV cutoff scale, Λ . Without any additional fields, the only *renormalizable* operator that involves SM fields is

$$\mathcal{L} \supset \frac{1}{2} \lambda \Phi^2 H^\dagger H , \quad (1)$$

where H is the Higgs doublet and λ is a dimensionless coupling. Such an operator can arise in an RS scenario for either IR brane-localized or bulk scalars Φ . For an IR brane-localized scalar (assuming the Higgs is also IR localized), the corresponding operator is

$$\mathcal{L}_5 \supset -\delta(L - y) \frac{1}{2} \lambda \Phi^2 H^\dagger H . \quad (2)$$

For a bulk scalar Φ the operator Eq. (1) can be induced from a non-renormalizable operator (to be discussed in the following subsection). If the cutoff is at the TeV scale the effective coupling λ can easily be of order one, so that the following analysis applies.

The interaction in Eq. (1) can lead to the direct self-annihilation of Φ particles into a pair of Higgses, and also, if the annihilations occur after the electroweak phase transition, into pairs of SM gauge bosons and fermions through s -channel Higgs exchange. When the Φ mass is much larger than the Higgs mass, the direct annihilation into Higgses dominates (this includes annihilation into the Goldstone modes, hence the $W_L W_L$ and $Z_L Z_L$ channels). Annihilation into two Higgses in the limit that $M_\Phi \gg v_{EW}$ (with v_{EW} the Higgs VEV) gives in the non-relativistic

regime

$$\langle \sigma_{\Phi\Phi \rightarrow HHv} \rangle \approx \frac{\lambda^2}{16\pi m_\Phi^2}, \quad (3)$$

where v is the relative velocity of the annihilating particles, and the brackets denote thermal averaging.

Notice that other annihilation channels have to proceed through operators suppressed either by the cutoff scale Λ or by a loop factor. As we will argue in the next subsection, when the Φ particles propagate in the bulk of an RS scenario those channels might be relevant (and could even dominate depending on couplings) in the total self-annihilation cross section, and therefore in the determination of the relic density. However, for a conventional four-dimensional scalar (or for a brane-localized Φ in an RS scenario¹) all other channels are expected to give a relatively small contribution when the Φ mass is less than the cutoff scale. For instance, annihilation into SM fermions would proceed through operators that also involve the Higgs field, of the form $\Phi^2 H \bar{\psi}_1 \psi_2$, and are suppressed at least by order $(v_{EW}/\tilde{\Lambda})^2$, where v_{EW} is the Higgs vacuum expectation value and $\tilde{\Lambda} = \Lambda e^{-kL}$ is the warped down cutoff scale if in a 5D warped framework, or more generally the cutoff scale of the 4D theory. Decays into SM gauge bosons are also expected to be subdominant so long as the DM mass is less than the cutoff, even if the cutoff scale is low, and will be discussed in Subsection 3.1 in the context of DM indirect signals [see Eqs. (13) and (14) and ensuing discussion].

Under the assumption that the DM candidate is heavy (say 1 TeV or so) and is thermally produced, the DM relic abundance is controlled by Eq. (3). Taking into account only the annihilation into Higgses through the operator Eq. (1), and requiring that the observed DM abundance is completely accounted for by Φ particles, we can determine the coupling λ as a function of M_Φ from the WMAP constraint $\Omega_{DM} h^2 \approx 0.11$ [7] and

$$\Omega_{DM} h^2 \approx \frac{1.04 \times 10^9 \text{ GeV}^{-1} x_F}{M_P} \frac{1}{\sqrt{g_*} \langle \sigma v \rangle}, \quad (4)$$

where $M_P \approx 1.22 \times 10^{19}$ GeV is the Planck mass, $x_F = M_\Phi/T_F$, with T_F the freeze-out temperature, g_* is the effective number of relativistic degrees of freedom at freeze-out, and $\langle \sigma v \rangle$ is the thermally averaged annihilation cross section times relative velocity in units of GeV^{-2} . We have assumed that the Φ particles are thermally produced and remain in thermal

¹The operators discussed in Subsection 2.2 vanish for a brane localized Φ since always one of the chiralities of any bulk fermion Ψ vanishes on the brane.

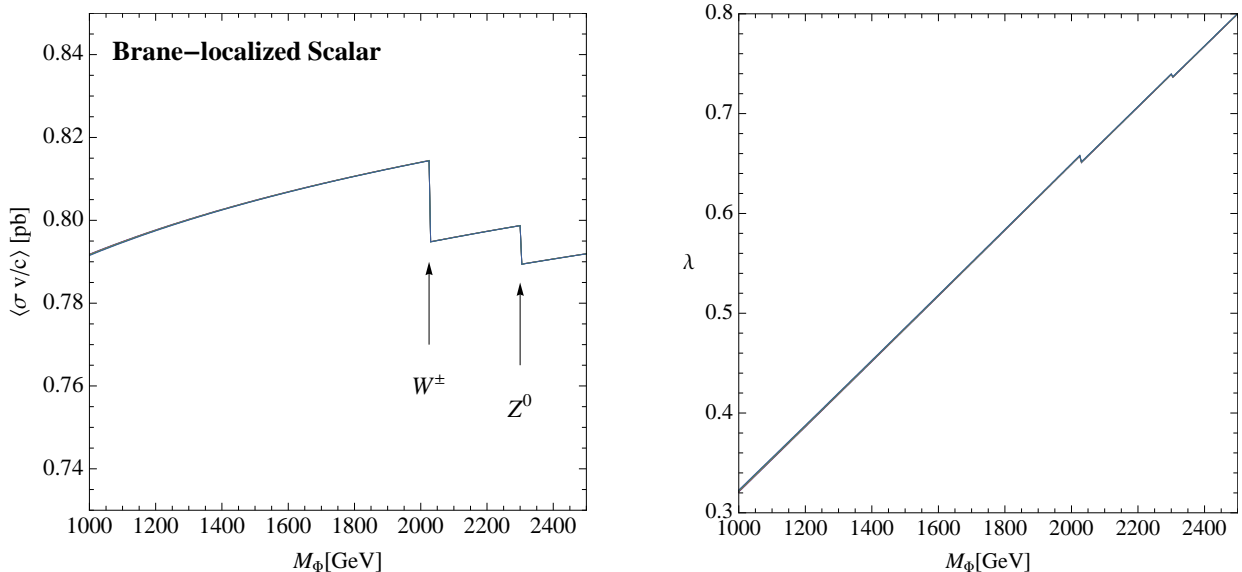


Figure 1: Left panel: annihilation cross section, $\langle\sigma_{\Phi\Phi\rightarrow HH\nu}\rangle$, for a brane-localized scalar in the non-relativistic regime as a function of M_Φ , imposing the WMAP constraint on the DM relic density. The arrows indicate the points where the freeze-out temperature ($\sim M_\Phi/25$) crosses the W^\pm and Z^0 thresholds. Right panel: the corresponding coupling λ , defined in Eq. (1), as a function of M_Φ .

equilibrium until freeze-out, which requires a coupling $\lambda > 10^{-8}$ [3]. For masses M_Φ in the few TeV range, λ is always of order unity, as shown in the right panel of Fig. 1, so the above assumption is self-consistently satisfied.

The required (non-relativistic) cross section as determined from the WMAP constraint to be $\langle\sigma v/c\rangle \approx 0.8$ pb and is shown in the left panel of Fig. 1 as a function of M_Φ , where the (weak) dependence of x_F on the cross section and the effective number of relativistic degrees of freedom g_* is included.² Throughout the range of interest we have $x_F \approx 25$, while g_* is of order 90. The above simple picture is rather generic for a stable TeV scale scalar field whenever the effects of higher-dimension operators can be neglected. However, when the scale suppressing the higher-dimension operators is near the TeV scale, other more exotic scenarios are possible. Such a situation, though less likely, could arise within the RS framework, and will be illustrated with a bulk scalar in the next subsection.

²The conversion factor from GeV^{-2} to pb is $0.3894 \times 10^9 \text{ GeV}^2 \text{ pb}$. Also, to convert the above cross section from pb into units of $\text{cm}^3 \text{ s}^{-1}$ [the CGS units for $\langle\sigma v\rangle$] one should multiply the number in pb by $(10^{-36} \text{ cm}^2) c \approx 3 \times 10^{-26} \text{ cm}^3 \text{ s}^{-1}$.

2.2 Bulk Singlet Dark Matter

Another natural possibility in a 5D warped background is that the DM candidate arises as the lightest KK mode of a bulk scalar. In order to be concrete, and simply for illustration purposes, we will assume in the following that there is a bulk SM singlet scalar obeying $(-, +)$ boundary conditions (Dirichlet on the UV brane, Neumann on the IR brane). In this case, the mass of the lightest KK mode is determined by only two dimensionless parameters, and can be easily below those of the gauge KK resonances (say around 1 TeV), as discussed in more detail in Appendix A. We also assume that the SM fermions and gauge fields arise from bulk fields.

The couplings to (an IR localized) Higgs field proceed now through the higher-dimension operator

$$-\delta(L-y)\frac{\lambda'}{2\Lambda}\Phi^2 H^\dagger H, \quad (5)$$

where Λ is the cutoff scale and λ' is a dimensionless coupling. After KK reduction, this induces a coupling of Φ s to Higgses similar to the one discussed in the previous subsection with the identification $\lambda = \lambda' f_{\Phi^{(1)}}^2 / (\Lambda L) \approx \lambda'(2k/\Lambda)$. Here $f_{\Phi^{(1)}} \approx \sqrt{2kL}$ is the $\Phi^{(1)}$ wavefunction evaluated on the IR brane, where $\Phi^{(1)}$ is the lightest scalar KK mode (the DM candidate). If this channel dominates the self-annihilation cross section, the relic density computation proceeds in exactly the same way as in the case of a brane-localized scalar discussed in the previous subsection. As was mentioned there, the observed relic abundance requires an effective 4D coupling λ of order one. Notice that for a bulk scalar, in spite of the suppression k/Λ , this is easily consistent with the NDA bound $\lambda' \lesssim 24\pi^3$ [8]; in fact, for $k/\Lambda \sim 1/10$ the fundamental coupling λ' is well into the perturbative regime, so that the computation is under theoretical control.

It is possible, however, that channels other than the annihilation into Higgses are important or even dominate, which could in principle differentiate between brane and bulk dark matter candidates. This scenario requires the value of λ' well below its NDA value with other couplings closer to what NDA would suggest. Since we are taking an agnostic attitude and are interested primarily in potential signatures and ways to identify the various possible scenarios, we consider this possibility next.

For this analysis it is useful to rewrite the annihilation cross section into Higgses as

$$\sigma_{\Phi\Phi \rightarrow HH\nu} \approx \frac{\lambda'^2}{4\pi\tilde{\Lambda}^2} \left(\frac{\tilde{k}}{M_\Phi} \right)^2, \quad (6)$$

where $\tilde{\Lambda} = \Lambda e^{-kL}$ is the warped down cutoff (of order a TeV) and similarly for $\tilde{k} = k e^{-kL}$. Now consider operators involving a 5D fermion field (giving rise to a SM fermion as its zero-mode), for instance

$$\frac{\lambda_\psi}{2\Lambda^2} \Phi^2 \bar{\Psi} \Psi , \quad (7)$$

where Ψ is the bulk fermion and λ_ψ is a dimensionless coupling. This operator leads to the annihilation of Φ particles into a SM fermion and one of its KK resonances, e.g.

$$\frac{\lambda_\psi \eta}{2\tilde{\Lambda}(\Lambda L)} (\Phi^{(1)})^2 \left[\bar{\psi}^{(1)} \psi^{(0)} + \bar{\psi}^{(0)} \psi^{(1)} \right] , \quad (8)$$

where $\psi^{(1)}$ is the first KK mode of the bulk fermion Ψ , and $\psi^{(0)}$ is its zero mode (with a well-defined chirality). The effective 4D coupling depends on the various extra-dimensional profiles through

$$\eta = \frac{1}{L} \int_0^L dy e^{k(y-L)} f_{\Phi^{(1)}}^2 f_{\psi^{(1)}} f_{\psi^{(0)}} , \quad (9)$$

where all the wavefunctions are normalized as in Eq. (32) of Appendix A.

Assuming that the channel $\Phi\Phi \rightarrow \psi^{(1)}\bar{\psi}^{(0)}$ is open, i.e. $M_{\psi^{(1)}} + m_{\psi^{(0)}} \leq 2M_\Phi$, the corresponding annihilation cross section is ³

$$\sigma_{\psi^{(1)}\bar{\psi}^{(0)}} v = \frac{N_c \lambda_\psi^2 \eta^2}{16\pi \tilde{\Lambda}^2 (\Lambda L)^2} \frac{(s - M_{\psi^{(1)}}^2)^2}{M_\Phi s^{3/2}} , \quad (10)$$

where $N_c = 3$ for quarks while $N_c = 1$ for leptons and, for simplicity, we neglected the zero-mode mass $m_{\psi^{(0)}}$. In the non-relativistic limit one has $\sigma_{\psi^{(1)}\bar{\psi}^{(0)}} v = a + b v^2 + \dots$, with

$$a = \frac{N_c \lambda_\psi^2 \eta^2}{8\pi \tilde{\Lambda}^2 (\Lambda L)^2} (1 - y)^2 , \quad b = \frac{N_c \lambda_\psi^2 \eta^2}{64\pi \tilde{\Lambda}^2 (\Lambda L)^2} (1 + 2y - 3y^2) , \quad (11)$$

where $y = M_{\psi^{(1)}}^2 / 4M_\Phi^2$. The related process $\sigma_{\psi^{(0)}\bar{\psi}^{(1)}} v$ is given by the same expression.

The magnitude of the annihilation cross sections into fermions depends strongly on the localization of the fermion zero-mode through the parameter η of Eq. (9). Recall that the fermion zero-mode wavefunctions are proportional to $e^{(1/2 - c_f)ky}$, where c_f parametrizes the 5D fermion mass in units of the AdS curvature scale k . The massive KK mode wavefunctions are all strongly localized near the IR brane. There are a number of distinct scenarios according to how flavor is generated:

³To simplify notation we will refer to the DM candidate $\Phi^{(1)}$ simply as Φ .

1. The SM fermion mass hierarchies arise from the exponential wavefunction localization and the overlap with an IR localized Higgs field. This scenario has the advantage that both calculable flavor changing effects (from KK gluon exchange), as well as non-calculable effects from flavor changing non-renormalizable operators, are significantly suppressed [9, 10, 11, 12]. One expects the third generation quarks (most likely the right-handed top) to couple most strongly to Φ .
2. All fermions share the same parameter c_f , and are localized close to the IR brane ($c_f < 1/2$), so that their couplings to Φ are sizable. Somewhat more generally, EW precision constraints allow different localization parameters for different fermions so long as those fermions having identical quantum numbers have nearly the same c_f (when IR localized; otherwise we are in scenario 1 above). In these scenarios, as-yet unspecified flavor-violating interactions would be necessary to explain the fermion mass hierarchies, while not generating dangerous FCNC effects from higher-dimension operators suppressed by the TeV scale.
3. Fermion mass hierarchies arise from localization in the extra dimension but the Higgs field is located on or near the UV brane (for example, if the Higgs mass is stabilized by supersymmetry (SUSY) and SUSY breaking is connected to the IR scale). In this case, the lightest fermions would be localized closer to the IR brane and have the largest couplings to Φ .

Among the fermion channels, Φ annihilates dominantly into the fermions closest to the IR brane, since the Φ wavefunction is localized near the IR brane. To calculate the annihilation rate, we need to estimate the expected size of these couplings, which can then be compared to the couplings to Higgses discussed above, or to the annihilation into gauge bosons (see Subsection 3.1).

For a fermion localized near the IR brane (localization parameter $c_f < 1/2$, but not very close to $1/2$), one finds $\eta \sim (1/5kL)(\sqrt{2kL})^3 \sqrt{(1-2c_f)kL} \approx \sqrt{\frac{1}{2} - c_f} kL$, where each KK wavefunction contributes a factor $\sqrt{2kL}$, the last factor corresponds to the c_f -dependent zero-mode wavefunction, and the factor $1/(5kL)$ is a measure of the region that contributes to the integral in Eq. (9).⁴ Compared to the annihilation into a pair of IR localized Higgses, Eq. (6), the annihilation into fermion and KK fermion is “suppressed” by order $(N_c/2)(\lambda_\psi/\lambda')^2(M_\Phi/\Lambda)^2(1/\Lambda L)^2$,

⁴The factor of $1/5$ is determined by comparison to the exact result, Eq. (9), and reproduces it within 30% for $-0.5 \lesssim c_f \lesssim 0.4$.

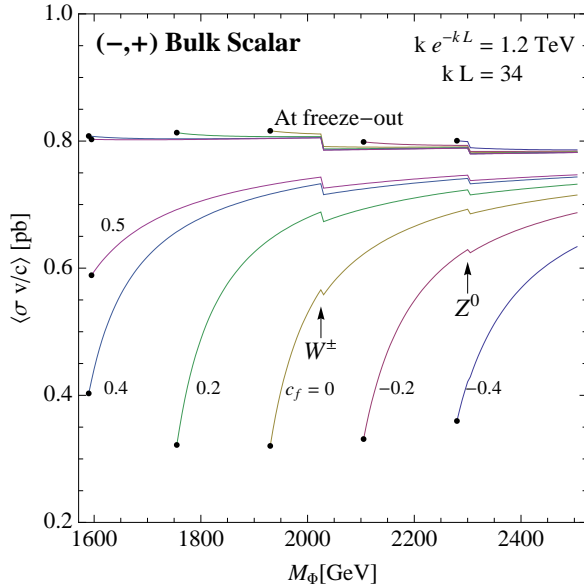


Figure 2: Annihilation cross section, $\langle \sigma_{\Phi\Phi \rightarrow \psi^{(0)}\psi^{(1)}v} \rangle$, for *bulk* DM, as a function of M_Φ , imposing the WMAP constraint on the DM relic density. The curves marked as “freeze-out” correspond to the annihilation cross section at the time of freeze-out (where the typical velocities were of order $v/c \sim \sqrt{2/25} \sim 0.3$). The lower curves correspond to the annihilation cross section in the ultra non-relativistic regime, as would be relevant for today’s conditions. The various curves correspond to different choices of the fermion localization parameter c_f that controls their masses and couplings. The arrows indicate the points where the freeze-out temperature ($\sim M_\Phi/25$) crosses the W^\pm and Z^0 thresholds. The curves are terminated (with black dots) when $\lambda_\psi = 24\pi^3$, which we define as the strong coupling regime (see text). We assume that $\Lambda = 8k$.

where it was assumed that the annihilation into fermions is not near threshold, and we used our estimate for η and take c_f of order one. The NDA estimate for λ_ψ is $24\pi^3$, which is the same as for λ' . However, the discussion after Eq. (5) indicates that a correct thermal relic abundance requires a much smaller coupling $\lambda' \lesssim \Lambda/(2k)$. Taking $\Lambda \lesssim 10k$, $M_\Phi \sim \tilde{k}$, $kL \approx 34$, one can see that the annihilation into an IR localized fermion and its lightest KK mode could dominate the annihilation cross section of Φ particles. Other operators that contribute to the self-annihilation cross section are expected to give subdominant contributions when $M_\Phi \ll \tilde{\Lambda}$. Nevertheless, the operators that lead to annihilation into gauge bosons can be interesting from the point of view of DM signals, and are discussed in subsequent sections.

We explore here the exotic picture where the Φ s are kept in thermal equilibrium dominantly by annihilation into a fermion and its lightest KK mode. For concreteness, we imagine here

scenario 1 discussed above, where the annihilation proceeds mainly into tops and its lightest KK resonance, but the same would hold in scenario 3 with one of the lightest leptons (either electrons or neutrinos) replacing the top. The results can also be applied in a straightforward way to scenario 2 with all fermions localized identically: one should just include a multiplicity factor $3 \times [3 \times 4 + 3] = 45$.

In scenario 1, the processes taken into account are $\Phi\Phi \rightarrow \bar{T}_L^{(1)}t_R$ and $\Phi\Phi \rightarrow T_L^{(1)}\bar{t}_R$, where $T^{(1)}$ is the first KK excitation of the RH top tower. The annihilation cross section depends on the lightest KK scalar and fermion masses M_Φ and $M_{T^{(1)}}$, which are both of order \tilde{k} . We fix \tilde{k} and obtain different values of M_Φ as described in Appendix A. The KK fermion mass has some dependence on c_t , which controls the localization of the t_R wavefunction. The overall strength of the cross section depends on the combination $\lambda_t/[\tilde{\Lambda}(\Lambda L)] = \lambda_t/[\tilde{k}(kL)](k/\Lambda)^2$. Assuming again that the Φ s account completely for the observed DM energy density, one can then fix the quantity⁵ $\lambda_t(k/\Lambda)^2$ using the WMAP result and Eq. (4) with $\langle\sigma v\rangle = a + 3b/x_F$ where the coefficients a and b are given in Eq. (11). In Fig. 2 we show the result for several values of the fermion localization parameter $c_f = c_t$ (for the RH top most likely c_t is close to 0). As expected, the annihilation cross section at freeze-out is $\langle\sigma v/c\rangle \approx 0.8$ pb. However, unlike the case of annihilation into scalar particles such as the Higgs field discussed in the previous subsection, both the a and b terms give a comparable contribution. As a result, the annihilation cross section at very low-temperatures, being dominated by the a term, is somewhat different from the cross section at freeze-out. This is relevant for annihilation under today's conditions, and is also shown in Fig. 2. The curves marked as ‘‘At freeze-out’’ correspond to the annihilation cross section at the time of Φ decoupling (when the typical velocities were $v/c \sim \sqrt{2/25} \sim 0.3$), while the curves in the lower part of the plot correspond to the annihilation cross section in the ultra non-relativistic regime, and correspond essentially to the a -term in Eq. (11). The behavior observed in these curves arises from the fact that as $\Delta M = 2M_\Phi - M_{T^{(1)}}$ approaches zero, the annihilation cross section vanishes. Specifically $a \sim \lambda_\psi^2(\Delta M)^2$ and $b \sim \lambda_\psi^2\Delta M$. Thus, near threshold the b term dominates, and the WMAP constraint requires the scaling $\lambda_\psi^2 \sim 1/\Delta M$. This explains why the annihilation cross section at very low temperatures decreases as M_Φ decreases (for fixed $M_{T^{(1)}}$), since $a \sim \lambda_\psi^2(\Delta M)^2 \sim 1/\lambda_\psi^2 \sim \Delta M$.

We terminate the curves at the point where the coupling λ_ψ reaches the strong coupling value given by NDA, $\lambda_\psi \sim 24\pi^3$, assuming $\Lambda \sim 8k$. As explained above this happens near the

⁵If Λ is defined as the scale where the $SU(3)_C$ gauge factor gets strong, then NDA gives $\Lambda L \sim 24\pi^3/(3g_s^2)$, where g_s is the 4D color coupling at the KK scale. For $kL \approx 34$ this corresponds to $\Lambda/k \approx 8$.

threshold for top-KK top production. The different curves are terminated at different points due to the c_t dependence of the KK fermion mass $M_{T^{(1)}}$. Thus, at strong coupling, λ_ψ cancels the volume suppression factor ΛL in Eq. (10) that arises from the fact that the operator Eq. (7) is suppressed by two powers of Λ . The fact that this channel then dominates over the Higgs pair production channel, in spite of arising from an operator of higher dimensionality can then be understood as due to the strong localization near the IR brane of the RH top quark, as encoded in the parameter η of Eq. (9) as well as the different values of the couplings of the associated operators. Away from threshold the coupling λ_ψ is a factor of 5-10 below the NDA value, so that the perturbative computation can be trusted.

It is therefore plausible that the annihilation into Higgses plays a subdominant role in the determination of the DM relic density. Of course it is straightforward to take both channels into account when they give a comparable contribution, but we will not do so here and turn instead to the possible DM signals of these scenarios. Note however that sizable brane-localized kinetic terms (that were not included in the above analysis) are known to lower the lightest KK masses significantly [13]. Thus, even for $\tilde{k} = 1.2$ TeV (as is suggested by the EW precision constraints as a lower bound on \tilde{k} , and as assumed in Fig. 2) the KK masses can easily be somewhat below a TeV. The qualitative behavior of the ultra non-relativistic cross section persists: it is of order 0.8 pb, and decreases by a factor of about two near the threshold for $\Phi\Phi \rightarrow T^{(1)}t$ annihilation (assuming that this is the main annihilation channel and that we are in the perturbative regime). Thus, in the following phenomenological analysis, we will allow a large range of KK masses and analyze the consequences for indirect detection.

3 Indirect Detection

Because the scalar couples to the Higgs, interactions relevant for direct-detection experiments are in principle possible [3]. However for the heavy scalars we are talking about the direct detection rate will be too low so we concentrate on indirect signals.

In this section we consider such possible signals from the DM candidates discussed in Section 2. We will argue that current experiments may be sufficiently sensitive to detect photons (or possibly positrons) from dark matter annihilation, most likely when non-renormalizable operators are present. We will present our bounds in terms of constraints on the cutoff scale Λ appearing in these operators, which in the RS context can be understood as being related to the fundamental gravity scale and more generally represents a scale of strong interactions.

We first concentrate on the most distinctive signals, $\Phi\Phi \rightarrow \gamma X$ and $\Phi\Phi \rightarrow e^+ X$, where the photon(s) and positron are produced from direct 2-body decays and have well-defined energies. We also consider the more exotic decay chain involving a KK lepton, which generally yields a continuous spectrum (even before propagation thorough the interstellar medium) except when this KK lepton is sufficiently heavy to be produced almost at rest so that the positrons that result from its decay have a spectral distribution similar to those of primary positrons.

Subsequently we will consider possibilities from the decay of the Higgs that would occur as a consequence of the dark matter-Higgs coupling.

3.1 Photons

We now consider possible photon signals arising from annihilating dark matter. For a continuous photon signal the total flux is obtained by integrating from some detector-dependent threshold energy up to the DM mass. In the scenarios discussed in Section 2 the continuous signal is likely too small to see but we comment on such decays at the end of this subsection.

We start by discussing the more interesting signal arising from the direct decays of the (slowly moving) DM particle into photons proceeding from higher dimension operators, in which case the final photon is nearly monoenergetic. Both decays into two photons and a photon and a Z could in principle contribute. The photon energy in the first process is approximately equal to M_Φ , while in the second process it is approximately $M_\Phi(1 - M_Z^2/4M_\Phi^2)$. For DM in the TeV range, the energy resolution of ACT's is not enough to resolve the two lines and they both appear to have energy essentially equal to M_Φ . It is therefore appropriate to add the two photon signals in the flux.

The annihilation of a SM singlet into photons can proceed via higher dimension operators which we write as

$$-\frac{e^2\kappa}{8\tilde{\Lambda}^2}\Phi^2 F_{\mu\nu}F^{\mu\nu} - \frac{e^2\kappa'}{4s_Wc_W\tilde{\Lambda}^2}\Phi^2 Z_{\mu\nu}F^{\mu\nu} , \quad (12)$$

where $F_{\mu\nu}$ and $Z_{\mu\nu}$ are the photon and Z gauge boson field strengths, s_W is the sine of the weak mixing angle, $\tilde{\Lambda}$ is the effective 4D cutoff scale, and κ, κ' are couplings of order one. The operators in Eq. (12) are the 4D effective operators induced by bulk or brane-localized operators, depending on whether Φ arises from a bulk field or is localized on the IR brane. In the RS framework the cutoff might be expected to be around the TeV scale and not far from the mass of Φ , so that the resulting annihilation into photons need not be extremely suppressed.

In the ultra non-relativistic limit (DM particle velocities in the galaxy are of order $v \sim 10^{-3}c$), the interaction terms in Eq. (12) give rise to the cross sections

$$\begin{aligned} \langle \sigma_{2\gamma} v/c \rangle &\approx \left(\frac{M_\Phi}{\tilde{\Lambda}} \right)^4 \frac{3\pi\alpha^2\kappa^2}{M_\Phi^2} \\ &\approx 0.2 \text{ pb} \left(\frac{1 \text{ TeV}}{M_\Phi} \right)^2 \left(\frac{M_\Phi}{\tilde{\Lambda}} \right)^4 \kappa^2, \end{aligned} \quad (13)$$

where α is the fine structure constant, and an annihilation cross section into γZ

$$\begin{aligned} \langle \sigma_{\gamma Z} v/c \rangle &\approx \left(\frac{M_\Phi}{\tilde{\Lambda}} \right)^4 \frac{6\pi\alpha^2\kappa'^2}{s_W^2 c_W^2 M_\Phi^2} \left(1 - \frac{M_Z^2}{4M_\Phi^2} \right) \\ &\approx 2.5 \text{ pb} \left(\frac{1 \text{ TeV}}{M_\Phi} \right)^2 \left(\frac{M_\Phi}{\tilde{\Lambda}} \right)^4 \kappa'^2. \end{aligned} \quad (14)$$

Notice that besides the enhancement in the γZ channel due to the gauge coupling (the factor $1/s_W^2 c_W^2 \approx 5.6$), there is an additional factor of 2 difference due to the identical particle nature of the final state photons in the 2γ channel. This factor is compensated by the explicit factor of 2 in Eq. (16) that accounts for the two photons in the final state.

The rates given in Eqs. (13) and (14) are small when the Φ mass is low due to the strong $(M_\Phi/\tilde{\Lambda})^4$ dependence. However, if $\tilde{\Lambda}$ is not much above M_Φ , ground based Cherenkov detectors can be sensitive to this signal. We will now interpret current bounds in terms of the implications for the cutoff scale $\tilde{\Lambda}$.

The differential photon flux from a direction that forms an angle ψ with the galactic plane is

$$\frac{d\Phi_\gamma}{d\Omega dE} = \sum_i \langle \sigma_i v \rangle \frac{dN_\gamma^i}{dE} \frac{1}{4\pi M_\Phi^2} \int_0^\infty dl \rho^2(r), \quad (15)$$

where $r^2 = l^2 + r_0^2 - 2lr_0 \cos \psi$, with $r_0 \approx 8.5$ kpc the distance from the Earth to the galactic center. The integration is along the line of sight, dl , and encodes the information about the DM distribution, assuming a spherical DM halo of energy density $\rho(r)$. The particle physics input enters through the thermally averaged cross section times relative velocity (for channels labeled by i) and the differential photon yield in channel i , dN_γ^i/dE where we add the $\gamma\gamma$ and γZ signals. We have

$$\Phi_\gamma = 5.66 \times 10^{-12} \text{ cm}^{-2} \text{ s}^{-1} \left[2 \left(\frac{\langle \sigma_{2\gamma} v/c \rangle}{1 \text{ pb}} \right) + \left(\frac{\langle \sigma_{\gamma Z} v/c \rangle}{1 \text{ pb}} \right) \right] \left(\frac{1 \text{ TeV}}{M_\Phi} \right)^2 \bar{J}(\Delta\Omega) \Delta\Omega, \quad (16)$$

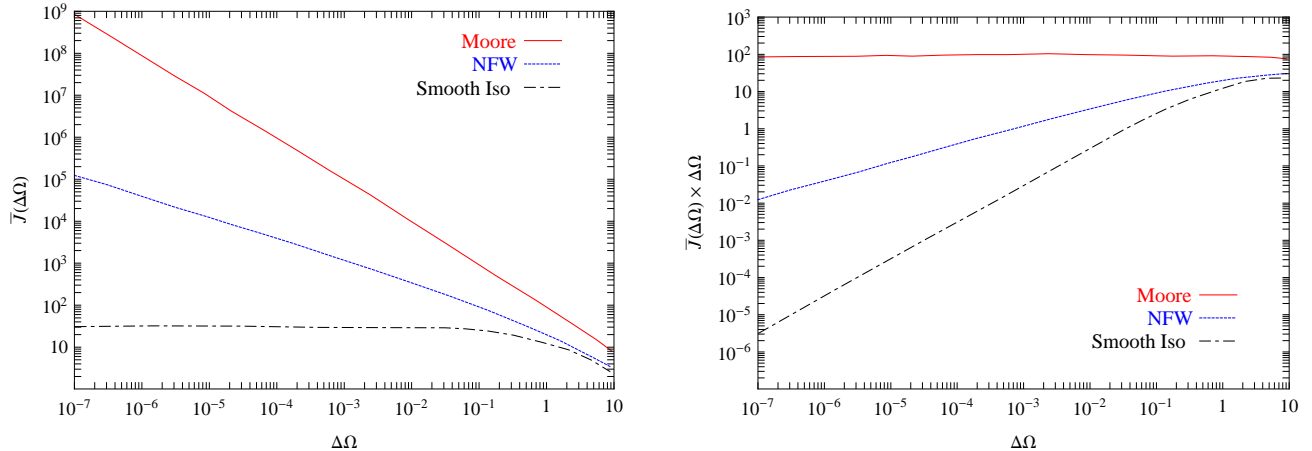


Figure 3: Left panel: $\bar{J}(\Delta\Omega)$ as a function of $\Delta\Omega$ for three different halo profiles (taken from Ref. [17]). Right panel: $\bar{J}(\Delta\Omega) \times \Delta\Omega$ as a function of $\Delta\Omega$.

where the factor of 2 corresponds to the two photons per decay in the 2γ annihilation channel, $\bar{J}(\Delta\Omega) \equiv (1/\Delta\Omega) \int_{\Delta\Omega} J(\psi) d\Omega$ integrates over the angular acceptance of the detector $\Delta\Omega$, and $J(\psi)$ is conventionally defined as

$$J(\psi) = \frac{1}{8.5 \text{ kpc}} \left(\frac{1}{0.3 \text{ GeV/cm}^3} \right)^2 \int_0^\infty dl \rho^2(r). \quad (17)$$

The quantity $\bar{J}(\Delta\Omega)$ depends on the DM halo profile and can vary over several orders of magnitude depending on the halo model, when looking towards the galactic center. It has been computed for several DM halo models, and as a function of $\Delta\Omega$ in [14]. In the left panel of Fig. 3 we reproduce $\bar{J}(\Delta\Omega)$ as a function of $\Delta\Omega$ for three different halo profiles: the Moore et. al. profile [15] (a rather cuspy profile), the widely used Navarro-Frenk-White (NFW) profile [16], and a smooth isothermal profile [17]. For reference we also show in the right panel the product $\bar{J}(\Delta\Omega) \times \Delta\Omega$ as a function of $\Delta\Omega$. The angular acceptance $\Delta\Omega$ depends on the experimental setup.

Several experiments exist that can search for photons from dark matter annihilation. Among the particle community, FERMI (formerly known as GLAST) has recently received a great deal of attention. FERMI is a satellite-based detector with excellent angular coverage (greater than about 2 sr) and fairly good energy resolution ($< 10\%$) [18]. FERMI should have a flux sensitivity of order 10^{-10} photons $\text{cm}^{-2} \text{s}^{-1}$ for photon energies between about 20 and 300 GeV (with decreasing sensitivity at lower energies and no sensitivity at higher energies).

Ground-based detectors, on the other hand, have much smaller angular coverage and worse energy resolution. However their flux sensitivity is similar to that of FERMI at around 50 GeV [19] and rapidly overtakes FERMI's sensitivity, depending on angular coverage, at higher energies. From the right panel in Fig. 3, and taking the NFW halo profile, we see that when $\Delta\Omega = 10^{-5}$ sr, a typical value used in HESS, one has $\bar{J}(\Delta\Omega) \times \Delta\Omega \approx 10^{-1}$, while for FERMI with $\Delta\Omega = 2$ one has $\bar{J}(\Delta\Omega) \times \Delta\Omega \approx 20$. Therefore, if HESS achieves only $\Delta\Omega = 10^{-5}$, it can be more sensitive than FERMI to the photon signal we discuss at energies of about 250 GeV [19] (near the end of FERMI's sensitivity range). Ground-based detection will be relatively more sensitive with a Moore profile and less so with an isothermal profile.

HESS and VERITAS could reach a larger angular coverage, since their fields of view (5° for HESS and 3.5° for VERITAS) correspond to $\Delta\Omega \sim 10^{-2}$ sr. If such angular acceptances are reached, and assuming an NFW profile so that $\bar{J}(\Delta\Omega) \times \Delta\Omega \approx 3$ (see Fig. 3), these ground-based detectors could overtake FERMI's sensitivity even at photon energies of about 100 GeV. Clearly the flux sensitivity is better for either of the ground based experiments⁶ for reasonable dark matter masses above about 100 GeV and the determining factor of which is better is likely to be the angular resolution.⁷

Of course, without knowing the dark matter profile, it makes sense to search in both satellite and ground-based experiments at low energies. However, it should be borne in mind that most dark matter models predict a monochromatic photon signal only at one loop so indirect detection is unlikely to be sufficiently sensitive to this type of signature of standard thermal dark matter. Supersymmetric dark matter annihilation into photons offers perhaps the best possible loop-suppressed scenario because the loop can be enhanced [21, 22] due to a reasonably large numerical factor and because for a higgsino dominated neutralino an enhancement in the loop diagram due to near degeneracy with an intermediate state can lead to a cross section that saturates with $1/m_W^2$ dependence (rather than suppression by the potentially bigger dark matter mass). This signal is potentially observable, however, only for light dark matter candidates for which the flux is big (and where FERMI is sensitive). Otherwise the cross section is too small.

We note that the direct signal we discuss is at higher energies since we assume a heavy dark matter candidate and therefore concentrate on ground-based experiments since they have

⁶VERITAS does not always point toward the galactic center, however, so the flux sensitivity in that regime is not guaranteed

⁷The sensitivity of ACTs to the photon signal at large $\Delta\Omega$ could be limited by the cosmic ray background, since subtracting the signal from a nearby region can have a significant effect for shallow profiles [20]. However, for more peaked profiles such as NFW, this is expected to be at most an order one effect.

$\Delta\Omega$	$\bar{J}(\Delta\Omega) \times \Delta\Omega$	$\tilde{\Lambda}$ [TeV] at $M_\Phi = 1$ TeV	$2\langle\sigma_{2\gamma}v\rangle + \langle\sigma_{\gamma Z}v\rangle$ [$\text{cm}^3 \text{s}^{-1}$]
10^{-5}	10^{-1} (NFW)	2	5.4×10^{-27} (1.8×10^{-1} pb)
10^{-3}	1 (NFW)	3.5	5.8×10^{-28} (1.9×10^{-2} pb)
any	10^2 (Moore)	11.3	5.3×10^{-30} (1.8×10^{-4} pb)

Table 1: Sensitivity of HESS or VERITAS to the cutoff scale $\tilde{\Lambda}$ for representative $\Delta\Omega$'s (NFW and Moore et. al. halo profiles). A DM candidate with mass $M_\Phi = 1$ TeV annihilating into monoenergetic 1 TeV photons is assumed. We assume $\kappa = \kappa' = 1$ (see text). The last column gives the thermally averaged annihilation cross section into photons for the corresponding $\tilde{\Lambda}$ (and for $M_\Phi = 1$ TeV).

better sensitivity. Although the number density of heavy dark matter particles is lower than that for lighter dark matter candidates, our prediction is a tree-level effect, albeit through a higher-dimension operator, and the cross section can be bigger than typical supersymmetric annihilation cross sections [21], which saturate at about $10^{-28} \text{ cm}^3 \text{ s}^{-1}$. For example, in the first row of Table 1 we see that for $\tilde{\Lambda} = 2$ TeV and $M_\Phi = 1$ TeV the annihilation cross section is $5.4 \times 10^{-27} \text{ cm}^3 \text{ s}^{-1}$.

For instance, for 1 TeV photons, HESS has a flux sensitivity of about $10^{-13} \text{ cm}^{-2} \text{ s}^{-1}$. Using $\Delta\Omega = 10^{-5}$ sr and taking the NFW halo profile, we see from the right panel in Fig. 3 that $\bar{J}(\Delta\Omega) \times \Delta\Omega \approx 10^{-1}$. The expected flux is then $\Phi_\gamma = 1.6 \times 10^{-12} \text{ cm}^{-2} \text{ s}^{-1} (1 \text{ TeV}/\tilde{\Lambda})^4$, which could be translated into a bound $\tilde{\Lambda} \gtrsim 2$ TeV (we also assumed $\kappa = \kappa' = 1$).⁸ Under the same assumptions, for 2.3 TeV photons HESS would put a bound $\tilde{\Lambda} \gtrsim M_\Phi \sim 2.3$ TeV. On the other hand, the sensitivity could in principle be bigger or smaller according to the dark matter profile. For example, for the rather peaked Moore et. al. profile, one has $\bar{J}(\Delta\Omega) \times \Delta\Omega \approx 10^2$ and the non-observation of a line at 1 TeV by HESS would correspond to a bound $\tilde{\Lambda} \gtrsim 11.3$ TeV. This is the expected scale for $\tilde{\Lambda}$ in several well-motivated scenarios that take into account the EW constraints [23, 24, 25, 26].

For HESS or VERITAS operating at $\Delta\Omega = 10^{-3}$ sr and using again the NFW halo model with $\bar{J}(\Delta\Omega) \times \Delta\Omega \approx 1$, the expected flux would be $\Phi_\gamma = 1.6 \times 10^{-11} \text{ cm}^{-2} \text{ s}^{-1} (1 \text{ TeV}/M_\Phi)^2 \times$

⁸For $M_\Phi = 1$ TeV and $\tilde{\Lambda} = 2$ TeV, the non-relativistic annihilation cross section into γZ is $\langle\sigma_{\gamma Z}v/c\rangle \approx 0.15$ pb, which is smaller than the cross section necessary for M_Φ to account for the observed DM energy density. The annihilation into two photons is smaller by a factor of about ten. The largest contribution to the annihilation cross section would come from either annihilation into Higgses or fermion-KK fermion pairs as discussed in Section 2, thus justifying the relic density computation discussed there.

$(M_\Phi/\tilde{\Lambda})^4$. For 1 TeV photons, HESS or VERITAS would be sensitive to $\tilde{\Lambda} \sim 3.5$ TeV. We summarize these observations in Table 1.

Ground-based Cherenkov detectors capable of operating at larger $\Delta\Omega$ can start probing theoretically interesting values of $\tilde{\Lambda}$ even for halo profiles not as peaked as the Moore et. al. profile. From Fig. 3 we see that for $\Delta\Omega \sim 1$, several halo profiles converge to $\bar{J}(\Delta\Omega) \times \Delta\Omega \approx 10$. An additional factor of 6 improvement in the flux sensitivity would then make scales $\tilde{\Lambda} \sim 10$ TeV accessible. Of course, larger $\Delta\Omega$ means also larger background, but hopefully the very characteristic line signal can be extracted if there are enough events (see Ref. [17]).

We finally mention the possibility of observing photons from Higgs decays (assuming that the main channel for DM annihilation is into Higgses, as in Subsection 2.1, so that $\langle\sigma_{HH}v\rangle \approx 0.8$ pb). For instance, for a SM-like Higgs with mass around $m_h = 135$ GeV, the branching fractions into $\gamma\gamma$ or $Z\gamma$ are of order 10^{-3} each. The photons from these channels present a flat spectrum between $E_{\min}^{\gamma\gamma} = \frac{1}{2}M_\Phi(1 - \beta)$ and $E_{\max}^{\gamma\gamma} = \frac{1}{2}M_\Phi(1 + \beta)$ for the $\gamma\gamma$ signal, or between $E_{\min}^{Z\gamma} = \frac{1}{2}M_\Phi(1 - m_Z^2/m_H^2)(1 - \beta)$ and $E_{\max}^{Z\gamma} = \frac{1}{2}M_\Phi(1 - m_Z^2/m_H^2)(1 + \beta)$ for the $Z\gamma$ signal. Here $\beta = \sqrt{1 - m_H^2/m_\Phi^2}$ is the velocity of the Higgs in the DM rest frame.

We show in Fig. 4 the total flux integrated from a threshold energy $E_{\text{th}} = 50$ GeV up to $E_{\max}^{\gamma\gamma}$, as a function of M_Φ . Here we optimistically assume $\bar{J}(\Delta\Omega) \times \Delta\Omega = 10^2$ as would be appropriate for the Moore profile though of course with other profiles the signal would be smaller. ACTs such as HESS or VERITAS would be sensitive to such a signal, but if the halo profile is less peaked or if the Higgs branching fraction into photons is smaller, this continuous signal becomes challenging. Nonetheless since this is a generic prediction of this type of model that doesn't rely on higher-dimension operators exploring the possibility of detecting such a signal is extremely worthwhile.

3.2 Positrons

Recently there has been intriguing evidence for an excess positron signal at energies up to about 80 GeV [27]. Clearly it is of interest to determine whether such positrons can arise from dark matter annihilation. We do not anticipate that heavy dark matter particles will explain this excess, since a positron signal, if it exists, will be concentrated at higher energies.

Nonetheless it is of interest to explore this positron signal to see how it compares to background and to see whether in principle the signal could be detectable at high energies. We also briefly consider lighter particles (with less theoretical motivation in our context of strongly interacting TeV scale physics) with similar interactions to KK dark matter particles and find

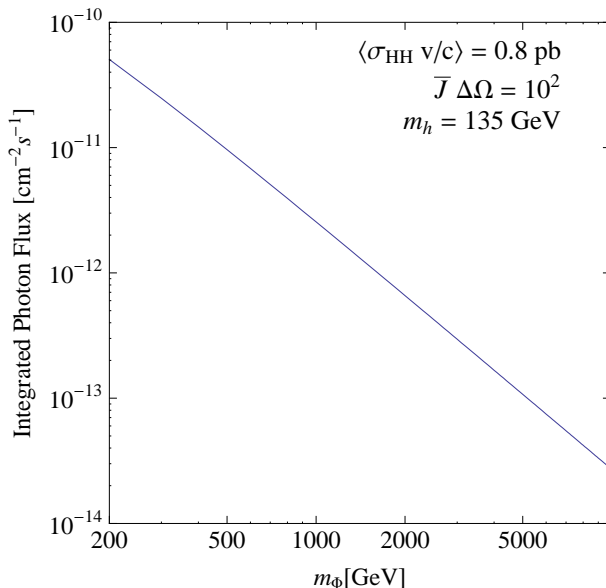


Figure 4: Integrated photon flux from $\Phi\Phi \rightarrow HH$ and $H \rightarrow \gamma\gamma$ or $H \rightarrow Z\gamma$, as a function of M_Φ . We assume that the branching fractions for these decay modes are 10^{-3} and take $\bar{J}(\Delta\Omega) \times \Delta\Omega = 10^2$.

that even without a big boost factor annihilations of ~ 100 GeV dark matter matches the PAMELA data.

With this in mind, we note that for the bulk scalar fields discussed in Subsection 2.2, other operators involving SM fields can be interesting from the point of view of DM signals, besides the operators leading to direct annihilation of the Φ particles into photons discussed in the previous subsection. Specifically, the higher-dimension operators of the type Eq. (8), coupling a pair of Φ s to an electron and its lowest KK mode, can lead to an interesting positron signal. The dominant annihilation channel involves the fermions closest to the IR brane (we discussed in Subsection 2.2 how the DM relic density can be determined by the annihilation into a SM fermion and one of its KK modes).

In Subsection 2.2 we defined three scenarios that differ on how the fermions are localized in the extra dimension. Of these, the most favorable one to obtain a sizable positron signal from DM annihilation is scenario 3. But we will see that only the electrons need to be somewhat localized near the IR brane for the positron signal to be interesting, and this can occur in scenario 2 as well.⁹ Note also that the positron signal is sensitive to the *local* DM distribution

⁹A hybrid case (of scenarios 1 and 2) with one of the lepton chiralities localized somewhat near the IR

(and not very much to how peaked the DM halo is at the galactic center). It is common to parameterize the effects of DM inhomogeneities by an (energy-independent) “boost” factor $B = \langle \rho^2 \rangle / \langle \rho \rangle^2$. Studies of such enhancements for gamma rays indicate that the boost factor might be as large as order 10 [28]. Therefore, the positron signal can receive an enhancement compared to the case of a smooth DM density distribution, though the likely size of this enhancement is not expected to be very large.

With this understanding we proceed to estimate the signal from direct annihilation into a positron and a KK mode. The produced positron has a well-defined energy that depends on the DM and KK fermion masses, M_Φ and $M_{e^{(1)}}$: $E_{e^+}^{\text{prim.}} = (4M_\Phi^2 - M_{e^{(1)}}^2)/4M_\Phi$. Besides these primary monoenergetic positrons, we also consider the secondary positrons arising from the annihilation of Φ particles into an electron (neutrino) and a positron KK mode followed by the decay of the associated KK lepton into a positron and a Z (W) gauge boson.¹⁰ When the KK lepton $l^{(1)} = e^{(1)}$ or $\nu^{(1)}$ has a mass slightly below $2M_\Phi$ (about the threshold for DM annihilation into lepton and KK lepton), it is produced nearly at rest and the resulting positron from its decay has a relatively well-defined energy. In detail, the energy of the KK lepton produced in DM annihilation is $E_{l^{(1)}} = (4M_\Phi^2 + M_{l^{(1)}}^2)/4M_\Phi$, while its momentum is $p = (4M_\Phi^2 - M_{l^{(1)}}^2)/4M_\Phi$. For the two-body decays $e^{(1)} \rightarrow Ze$ or $\nu^{(1)} \rightarrow We$, one finds the typical flat spectral distribution

$$f_2(E_0) = \begin{cases} (E_{l^{(1)}}\beta_{l^{(1)}})^{-1} & E_- \leq E_0 \leq E_+ \\ 0 & \text{otherwise} \end{cases}, \quad (18)$$

where E_0 is the positron energy. Neglecting the masses of the decay products, the maximum positron energy is $E_+ = \frac{1}{2}E_{l^{(1)}}(1 + \beta_{l^{(1)}}) = M_\Phi$, while the minimum positron energy is $E_- = \frac{1}{2}E_{l^{(1)}}(1 - \beta_{l^{(1)}}) = M_{l^{(1)}}^2/4M_\Phi$. Here $\beta_{l^{(1)}} = p/E_{l^{(1)}} = (4M_\Phi^2 - M_{l^{(1)}}^2)/(4M_\Phi^2 + M_{l^{(1)}}^2)$ is the velocity of the KK lepton (in the rest frame of Φ). Notice that the upper endpoint is determined by

brane and the opposite chirality localized near the UV brane (to generate the small lepton masses by the exponential wavefunction suppression) also falls in this category. For instance if $c_{l_R} \approx 0.4$ while $c_{t_R} \approx 0$, we have $\eta_{t_R}/\eta_{l_R} \approx [(1 - 2c_{t_R})/(1 - 2c_{l_R})]^{1/2} \sim 2$, where the η parameters were defined in Eq. (9). Therefore, the annihilation into positrons can plausibly be suppressed compared to the dominant top channel by only a factor $\sim 4N_c \sim 10$, if the unknown dimensionless coefficients λ_e and λ_t in Eq. (7) are assumed to be comparable.

If only the RH top and the RH leptons are localized near the IR brane and one neglects other annihilation channels, the thermal relic density computation implies $\langle \sigma_{e^{(1)}e} v/c \rangle = \langle \sigma_{\mu^{(1)}\mu} v/c \rangle = \langle \sigma_{\tau^{(1)}\tau} v/c \rangle \approx 0.06$ pb and $\langle \sigma_{t^{(1)}t} v/c \rangle \approx 0.6$ pb.

¹⁰The decays of the KK lepton into Higgs are suppressed by the electron Yukawa coupling. For gauge KK masses of order 3 TeV, the main decay channels of the KK lepton involve Z or W (through EWSB mixing of the Z/W with its KK modes, as opposed to mixing of the lepton and its KK modes). When the lepton is an $SU(2)$ doublet we have $\Gamma(e^{(1)} \rightarrow Ze)/\Gamma(\nu^{(1)} \rightarrow We) \approx (m_Z^4/m_W^4)(T^3 - s_W^2 Q)^2/c_W^2$, leading to $\text{BR}(\nu^{(1)} \rightarrow We) \approx 75\%$ and $\text{BR}(e^{(1)} \rightarrow Ze) \approx 25\%$. Similarly, the $SU(2)$ singlet KK positron decays dominantly into Ze^+ .

the DM mass only, and that in the limit $M_{l(1)} \rightarrow 2M_\Phi$ one has $f_2(E_0) \rightarrow \delta(E_0 - M_\Phi)$. Further decays of the W s and Z s lead to additional positrons that have a softer spectrum and give a subdominant contribution due to the small branching fractions involved. We do not include positrons from W or Z decay in the following analysis. Note also that primary and secondary electrons with the exact same characteristics as the positrons above are also produced.

The positron energy is distorted as it propagates through the interstellar medium before detection. In general, for an initial spectral distribution $f_i(E_0)$, normalized according to $\int_0^\infty dE_0 f_i(E_0) = 1$, the differential positron flux at the solar position is obtained from

$$\frac{d\Phi_{e^+}}{d\Omega dE} = \frac{B\rho_0^2}{m_\Phi^2} \sum_i \langle \sigma_i v \rangle B_{e^+}^i \int dE_0 f_i(E_0) G(E_0, E) , \quad (19)$$

where ρ_0 is the average DM mass density, B is the boost factor, $\langle \sigma_i v \rangle$ is the i -th channel thermally averaged (ultra non-relativistic) DM annihilation cross section times relative velocity, $B_{e^+}^i$ is the corresponding branching fraction into positrons, and $G(E_0, E)$ is a Green function that includes the details of the DM mass distribution in the galactic halo, takes into account the propagation of the positrons through the interstellar medium in the galaxy, and describes how their energy E is shifted under diffusion, various spatially and energy-dependent energy loss mechanisms, reacceleration, etc. The direct annihilation into positrons plus their lightest KK mode simply corresponds to $f(E_0) = \delta(E_0 - E_{e^+}^{\text{prim.}})$, while secondary positrons arising from the decay of the KK lepton are described by Eq. (18).

In Ref. [29], Moskalenko and Strong modeled the propagation of positrons through the interstellar medium for several galactic halo DM mass distributions. They provided a simple parameterization for the Green function that reproduces the more detailed simulation¹¹ to within 10%:

$$10^{-25} E^2 G(E_0, E) = 10^{a(\ln E)^2 + b \ln E + c} \theta(E - E_0) + 10^{w(\ln E)^2 + x \ln E + y} \theta(E_0 - E) , \quad (20)$$

where $G(E_0, E)$ is given in units of $\text{cm sr}^{-1} \text{GeV}^{-1}$, E is the local positron energy in GeV, and the coefficients a , b , c , w , x and y are functions of E_0 (the initial positron energy) that are tabulated in Tables II and III of Ref. [29]. For definiteness, we consider the ‘‘isothermal’’ model, which is characterized by a spherically symmetric DM mass distribution given by

$$\rho(r) = \rho_0 \frac{r_c^2 + R_\odot^2}{r_c^2 + r^2} , \quad (21)$$

¹¹The code used in the simulation aims at reproducing simultaneously observational data related to cosmic ray origins and propagation such as: direct measurements of nuclei, antiprotons, electrons and positrons, as well as indirect measurements via γ rays and synchrotron radiation.

where r_c is the core radius and $R_\odot = 8.5$ kpc is the solar distance to the galactic center (the parameters r_c and ρ_0 are obtained by fitting to the rotation curve, and for the isothermal model $r_c = 2.8$ kpc and $\rho_0 = 0.43$ GeV cm⁻³). We use a galactic halo size of $z_h = 10$ kpc, which is on the upper limit of the 4 – 10 kpc range favored by the analysis in [29].

The local positron flux then takes the form

$$E^2 \frac{d\Phi_{e^+}}{d\Omega dE} = 2.7 \times 10^{-8} \left(\frac{\rho_0}{0.3 \text{ GeV/cm}^3} \right)^2 \left(\frac{1 \text{ TeV}}{m_\Phi} \right)^2 \sum_i \left(\frac{B \langle \sigma_i v/c \rangle}{1 \text{ pb}} \right) B_{e^+}^i F_i(E), \quad (22)$$

where the units on the r.h.s. are GeV cm⁻²s⁻¹sr⁻¹, and the dimensionless $F_i(E)$ is defined by

$$F_i(E) = 10^{-25} E^2 \int dE_0 f_i(E_0) G(E_0, E). \quad (23)$$

Experimental observations are commonly presented in the form of the positron fraction, $e^+/(e^- + e^+)$, where the electron and positron fluxes include both background and signal. This quantity has the advantage that systematic uncertainties cancel out. For the electron and positron background spectral distributions we use the simple parameterizations given in [30]:

$$\begin{aligned} \left(\frac{d\Phi_{e^-}}{d\Omega dE} \right)_{\text{prim. bkg}} &= \frac{0.16 E^{-1.1}}{1 + 11 E^{0.9} + 3.2 E^{2.15}}, \\ \left(\frac{d\Phi_{e^-}}{d\Omega dE} \right)_{\text{sec. bkg}} &= \frac{0.70 E^{0.7}}{1 + 110 E^{1.5} + 600 E^{2.9} + 580 E^{4.2}}, \\ \left(\frac{d\Phi_{e^+}}{d\Omega dE} \right)_{\text{sec. bkg}} &= \frac{4.5 E^{0.7}}{1 + 650 E^{2.3} + 1500 E^{4.2}}, \end{aligned}$$

where E is in GeV and the units of the l.h.s are GeV⁻¹ cm⁻² s⁻¹ sr⁻¹.

In the following we envision a scenario in which the dominant DM annihilation channel is into pairs of electron/positron plus a KK mode, as could be expected in scenario 3 defined in Subsection 2.2. In this case, the WMAP relic abundance requires $\langle \sigma_{e^{(1)}e} v/c \rangle \approx 1$ pb. Somewhat more generally, the results are valid for $B \times \langle \sigma_{e^{(1)}e} v/c \rangle = 1$ pb, where B is the boost factor. Since B is expected to be order a few, our results can illustrate situations where the electron/positron channel is one among a few dominant annihilation channels (e.g. if the other lepton channels are equally important).

In the left panel of Fig. 5 we show the expected positron fraction signal, assuming DM masses $M_\Phi = 500$ GeV and $M_\Phi = 2$ TeV. We also include the secondary positrons arising from the decay of the KK lepton, assuming $M_{e^{(1)}} = M_\Phi$. Interestingly, there is a rather clear

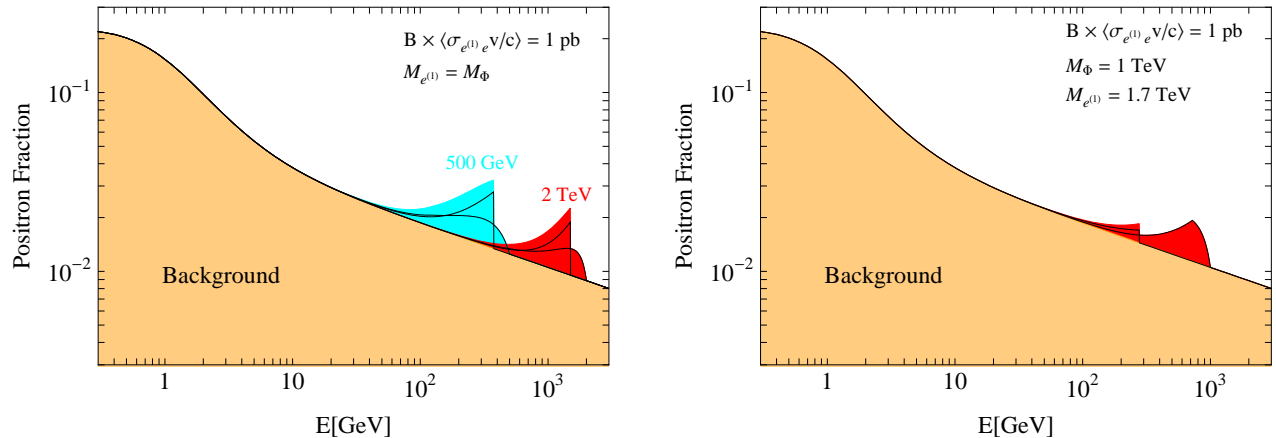


Figure 5: Left panel: positron fraction including the primary positrons/electrons from the annihilation $\Phi\Phi \rightarrow e^\pm e^{(1)}$ and the secondary positrons/electrons from the annihilation $\Phi\Phi \rightarrow l^{(1)}l^{(0)}$, followed by a two-body decay $l^{(1)} \rightarrow e^\pm X$. We show the spectra for two DM masses, $M_\Phi = 500$ GeV and $M_\Phi = 2$ TeV, assuming that $M_{e^{(1)}} = M_\Phi$ and a boost factor such that $B \times \langle\sigma_{e^{(1)}e}v/c\rangle = 1$ pb, with $\rho_0 = 0.3$ GeV/cm³. The solid lines represent the individual contributions from primary and secondary production. Right panel: positron fraction for $M_\Phi = 1$ TeV and $M_{l^{(1)}} = 0.85 \times (2M_\Phi) = 1.7$ TeV showing clear peaks at $E_{e^+}^{\text{prim.}} = (4M_\Phi^2 - M_{e^{(1)}}^2)/4M_\Phi$ and near M_Φ (the endpoint is exactly at M_Φ).

peak above background that could be observable in the sub TeV range. A moderate boost factor would make such a feature even more prominent. In the right panel of Fig. 5 we show another example where $M_{e^{(1)}} = 0.85 \times 2M_\Phi$ is closer to threshold. This case exhibits more clearly the two peaks discussed above, one at $E_{e^+}^{\text{prim.}}$ from the primary positrons and another near M_Φ for the secondary positrons from the KK lepton decay. As remarked above, the upper endpoint gives a direct measurement of M_Φ . The first peak then gives information about the KK lepton mass. With a handle on the DM and KK fermion masses it would be possible to get information about the effective cutoff scale $(\lambda_e/\Lambda L)^{-1}\tilde{\Lambda}$ [see coefficient a in Eq. (11)], modulo the uncertainty associated with the local DM energy density (since these high-energy positrons come from distances of at most a few kpc, the dependence on the DM halo model is expected to be milder).

There seems to be evidence in several experiments for an excess in the positron flux in the tens of GeV energy range (HEAT [31], AMS-01 [32]), with the PAMELA satellite experiment supporting this excess up to energies of about 80 GeV [27]. As has been emphasized recently [33, 34, 35] the observed fluxes are larger than what would be expected from thermal WIMPs when

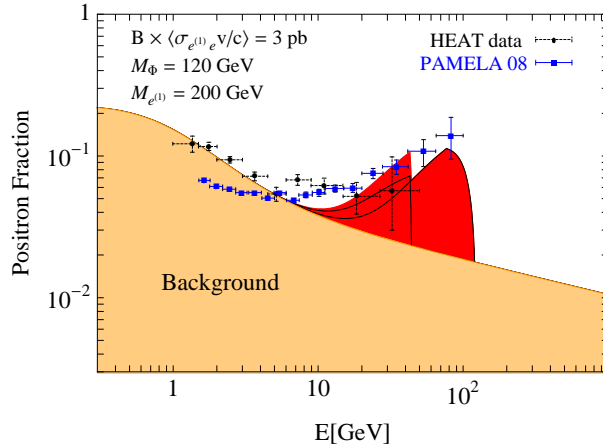


Figure 6: Positron fraction due to positrons from a 120 GeV DM particle annihilating into $ee^{(1)}$, where $e^{(1)}$ is a heavy electron of mass $M_{e^{(1)}} = 200$ GeV. The lower energy peak arises from direct annihilation into a positron (plus heavy lepton), while the higher-energy peak arises from the direct decay of the heavy lepton into a positron (plus a gauge boson). Further positrons from the W 's or Z 's produced in the heavy lepton decay are not included and would add a softer contribution. We assume $B \times \langle \sigma_{e^{(1)}e} v/c \rangle = 3$ pb.

these lead to positrons mainly through the decays of their annihilation products (e.g. W 's).¹²

Nonetheless, it is interesting to note that a DM candidate with a mass of about 100 GeV annihilating primarily into electrons/positrons can explain the observed positron excess with a boost factor of order unity. Although such low masses are not expected in our scenario, we show in Fig. 6 the positron signal from the annihilation of a 120 GeV DM candidate into a positron and a “heavy vector-like electron” of mass $M_{e^{(1)}} = 200$ GeV. We show the HEAT data and the recently released PAMELA data, which shows a clear increase with energy of the positron fraction up to energies of at least 80 GeV [27]. However, the ATIC-2 balloon experiment [38] also indicates an excess in the total electron plus positron flux extending up to energies of about a TeV, which would not be explained by the self-annihilation into electrons/positrons of such a light DM candidate. Antiprotons produced in decays of the heavy electron (via W gauge bosons) may also conflict with the non-observation of an antiproton excess in the PAMELA \bar{p}/p data [39].

Of course the above observations hold only for a light dark matter particle of order 100 GeV.

¹²However, the presence of a relatively long range force among the DM particles can lead to an enhancement of several orders of magnitude in the annihilation cross section at very low velocities, which can account for these observations in certain dark matter models [34, 36, 37]. Our DM candidate, having only non-renormalizable interactions, does not fall into this category.

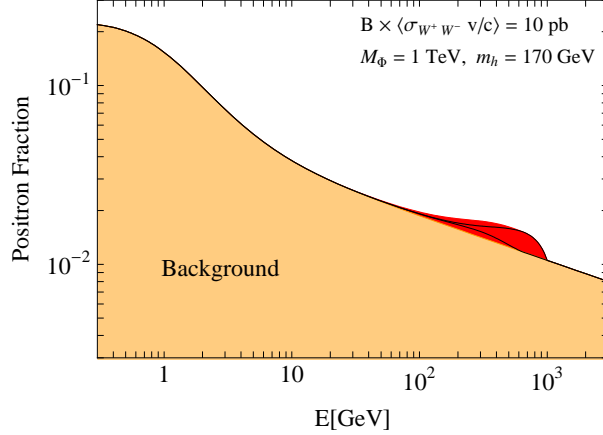


Figure 7: Positron fraction when $\Phi\Phi \rightarrow H^\dagger H$ (including longitudinal gauge bosons) dominates the DM annihilation cross section. We include the secondary positrons/electrons from the annihilation $\Phi\Phi \rightarrow W_L^+ W_L^-$ and the tertiary positrons/electrons from the annihilation $\Phi\Phi \rightarrow hh \rightarrow 4W$, assuming $m_h = 170$ GeV. Only two-body W decays into positrons/electrons are included. We take $M_\Phi = 1$ TeV and $B \times \langle\sigma_{W+W^-} v/c\rangle = 10$ pb, with $\rho_0 = 0.3$ GeV/cm³. The solid lines represent the individual contributions from secondary and tertiary production, with the latter having a softer spectrum.

For the range of masses expected in our scenario (around 1 TeV), the proton flux is sufficiently suppressed, but the positron excess below about 80 GeV would not be explained. However, the signal can exceed the background at high energy which would be interesting if experiments can attain the required sensitivity.

We close this subsection by coming back to the case of a scalar DM candidate that decays dominantly into Higgses, as discussed in Subsection 2.1, and comment on the associated positron signal. The annihilation cross section Eq. (3) corresponds to the processes $\Phi\Phi \rightarrow W_L W_L$, $\Phi\Phi \rightarrow Z_L Z_L$ and $\Phi\Phi \rightarrow hh$ in the large M_Φ limit. In this limit we have $\sigma(\Phi\Phi \rightarrow W_L W_L) \approx 2\sigma(\Phi\Phi \rightarrow Z_L Z_L) \approx 2\sigma(\Phi\Phi \rightarrow hh)$. Further decays of the W s, Z s and Higgses can result in energetic positrons. We consider here the case $m_H = 170$ GeV with a SM branching fraction $\text{BR}(H \rightarrow W^+ W^-) \approx 1$, and compute the spectrum of *secondary* positrons from $\Phi\Phi \rightarrow 2W/Z \rightarrow e^+ X$ and of *tertiary* positrons from $\Phi\Phi \rightarrow hh \rightarrow 4W \rightarrow e^+ X$. We do not include positrons from processes further down the decay chain.

The cross sections times branching fractions (including the positron multiplicities) to be used in Eq. (22) are $\langle\sigma_{W+W^-} v\rangle \times \text{BR}(W \rightarrow e\nu)$, $2 \times \langle\sigma_{ZZ} v\rangle \times \text{BR}(Z \rightarrow e^+ e^-) \approx \langle\sigma_{W+W^-} v\rangle \times \text{BR}(Z \rightarrow e^+ e^-)$, and $2 \times \langle\sigma_{HH} v\rangle \times \text{BR}(H \rightarrow W^+ W^-) \times \text{BR}(W \rightarrow e\nu) \approx \langle\sigma_{W+W^-} v\rangle \times \text{BR}(W \rightarrow e\nu)$,

respectively, where $\text{BR}(W \rightarrow e\nu) \approx 0.11$ and $\text{BR}(Z \rightarrow e^+e^-) \approx 0.036$. In Fig. 7, we show the positron fraction for $M_\Phi = 1$ TeV and $B \times \langle \sigma_{W+W^-} v/c \rangle = 10$ pb, which corresponds to a boost factor $B \approx 20$. We conclude that such a signal would be visible above background only for rather large boost factors. In particular, such a scenario can also not explain the observed positron excess reported at lower energies.

4 Conclusions

We considered a simple scenario for scalar DM of mass around 1 TeV in the context of non-renormalizable theories with a cutoff near the TeV scale. Such a possibility arises naturally in extra-dimensional models that address the hierarchy problem, such as the Randall-Sundrum scenario but could also arise from other strongly interacting TeV-scale theories. The thermal relic density can be determined either by renormalizable or non-renormalizable interactions. Such dark matter particles are clearly more challenging to detect but can conceivably yield observable gamma ray signals at current detectors and might ultimately yield observable positrons.

A monochromatic gamma ray line signal arises from the direct annihilation via nonrenormalizable operators of the DM particle Φ into photons. For a cutoff scale of up to about 10 TeV, such a signal can be larger than the signal from a typical one-loop induced direct coupling to photons. We also point out that the monochromatic signal associated with non-renormalizable operators is likely observable in currently operating ground-based experiments, and could be used to probe the cutoff scale up to several TeVs.

We also consider secondary photons from Higgs decay in the annihilation $\Phi\Phi \rightarrow HH$, and find that this continuous signal can be observable if the DM halo is relatively peaked at the galactic center. Secondary or tertiary positrons can also be produced in the decays of Higgses or longitudinally polarized gauge bosons, but the positron flux is likely too small to be observable above background.

It is also possible to have more exotic scenarios where the annihilation cross section is dominated by the non-renormalizable interactions, as opposed to the dimension-4 coupling of Φ to the SM Higgs field. In the extra-dimensional context one could have annihilations into a SM fermion and the associated KK fermion dominating the total annihilation cross section. If the leptonic channels are dominant, it is possible to have an observable positron signal in the 100 GeV to 1 TeV range with a boost factor of order one. Such a signal would typically present two peaks, due to the heavy lepton involved. However, the expected flux is too small to account

for the positron excess reported by HESS/AMS-01 and the PAMELA satellite experiment. Nevertheless, we find it promising that indirect searches in the sub-TeV range can be sensitive to cutoff scale physics.

Acknowledgements

We would like to thank Douglas Finkbeiner, Fiona Harrison, Sterl Phinney and Neil Weiner for useful conversations. E.P. is supported by DOE under contract DE-FG02-92ER-40699. L.R. is supported by NSF grant PHY-0556111.

A Bulk Scalars in an RS Background

We consider a bulk real scalar, Φ , propagating in the background [5]

$$ds^2 = e^{-2ky} \eta_{\mu\nu} dx^\mu dx^\nu - dy^2 , \quad (24)$$

where x^μ ($\mu = 0, 1, 2, 3$) are the 4D coordinates, and $0 \leq y \leq L$ parametrizes the fifth dimension. We assume that the scalar obeys $(-, +)$ boundary conditions, and consider the action

$$S = \int d^4x \int_0^L dy \sqrt{|g|} \frac{1}{2} \{ \partial_M \Phi \partial^M \Phi - M^2 \Phi^2 - \delta(y-L) m \Phi^2 \} , \quad (25)$$

where M and m are bulk and IR localized mass parameters, respectively. We do not write a localized mass on the UV brane, since the scalar is assumed to vanish at $y = 0$. We will parametrize these mass parameters in units of the curvature scale as

$$M^2 = \left[c_s^2 + c_s - \frac{15}{4} \right] k^2 , \quad (26)$$

$$m = \left[c_s - \frac{3}{2} + \delta \right] k . \quad (27)$$

For $\delta = 0$, the mass spectrum that follows coincides precisely with that of a fermion obeying $(-, +)$ b.c., where $c_f = c_s$ parametrizes the fermion bulk mass [40]. Our sign conventions are such that for $c_s < 1/2$ the lightest KK mode is exponentially localized near the IR brane, and when $c_s < -1/2$ its mass is exponentially smaller than the warped down curvature scale $\tilde{k} = k e^{-kL}$. We will see that the lightest eigenvalue can remain small for a wide range of values of the parameter δ defined in Eq. (27), and therefore the lightest scalar KK mode can be easily lighter than the SM gauge and fermion KK resonances.

The KK decomposition for Φ reads

$$\Phi(x^\mu, y) = \frac{e^{ky}}{\sqrt{L}} \sum_{n=1}^{\infty} \phi^n(x^\mu) f_n(y) , \quad (28)$$

where we pulled out an explicit factor e^{ky} for convenience, and the KK wavefunctions obey

$$\partial_y^2 f_n - 2k\partial_y f_n - (3k^2 + M^2)f_n = -e^{2ky} m_n^2 f_n , \quad (29)$$

and satisfy the b.c.:

$$f_n(0)|_{y=0} = 0 , \quad \partial_y f_n|_{y=L} = -(k+m)f_n(L) . \quad (30)$$

The solutions can be written in terms of Bessel functions as

$$f_n(y) = A_n e^{ky} \left[J_{|c_s + \frac{1}{2}|} \left(\frac{m_n}{k} e^{ky} \right) + b Y_{|c_s + \frac{1}{2}|} \left(\frac{m_n}{k} e^{ky} \right) \right] , \quad (31)$$

where A_n is a normalization constant, determined from

$$\frac{1}{L} \int_0^L dy f_n(y) f_m(y) = \delta_{nm} , \quad (32)$$

and

$$b = -\frac{J_{|c_s + \frac{1}{2}|} \left(\frac{m_n}{k} \right)}{Y_{|c_s + \frac{1}{2}|} \left(\frac{m_n}{k} \right)} . \quad (33)$$

The eigenvalues can be written as $m_n = x_n k e^{-kL}$, where the x_n solve

$$\frac{J_{|c_s + \frac{1}{2}|}(x_n e^{-kL})}{Y_{|c_s + \frac{1}{2}|}(x_n e^{-kL})} = \frac{x_n J_{|c_s + \frac{1}{2}|-1}(x_n) + (c_s + \frac{1}{2} - |c_s + \frac{1}{2}| + \delta) J_{|c_s + \frac{1}{2}|}(x_n)}{x_n Y_{|c_s + \frac{1}{2}|-1}(x_n) + (c_s + \frac{1}{2} - |c_s + \frac{1}{2}| + \delta) Y_{|c_s + \frac{1}{2}|}(x_n)} . \quad (34)$$

For $kL \gg 1$, the lowest solutions are approximately given by the vanishing of the numerator in the r.h.s of Eq. (34). We show the smallest eigenvalue in Fig. 8 as a function of δ , defined in Eq. (27), for several values of c_s [which parametrizes the bulk mass M^2 as in Eq. (26)]. This eigenvalue can be well approximated by

$$x_1 \approx \begin{cases} 2\sqrt{\frac{1}{2} - c_s} \sqrt{\frac{\delta}{2+\delta}} & c_s < -1/2 , \\ 2\sqrt{\frac{3}{2} + c_s} \sqrt{\frac{1+2c_s+\delta}{3+2c_s+\delta}} & c_s > -1/2 . \end{cases} \quad (35)$$

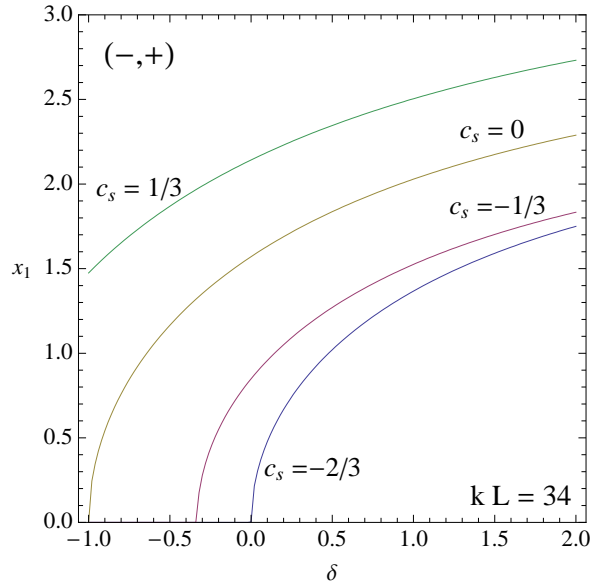


Figure 8: Lightest mass, $m_1 = x_1 k e^{-kL}$, for a bulk scalar obeying $(-, +)$ b.c., as a function of bulk and IR localized masses, parametrized by c_s and δ , as in Eqs. (26) and (27). Recall that for a KK gauge boson obeying $(+, +)$ b.c., $x_1 \approx 2.45$.

We see that for $\delta < \text{Min}\{0, -(1 + 2c_s)\}$, x_1^2 becomes negative and the corresponding mode is a tachyon. We will assume that we are in a region where no such instability arises. One should also keep in mind that for $\delta = 0$ and $c_s \approx -1/2$, Eq. (35) receives additional corrections not shown there. In this case, the smallest eigenvalue remains non-zero, becoming exponentially small for $c_s < -1/2$.

For Fig. 2 in the main text, we chose $c_s = -0.2$ and adjusted δ so as to reproduce the desired mass M_Φ . This determines the corresponding wavefunction and allows the computation of the relevant overlap integrals that determine the Φ couplings. Note, however, that the dependence on the choice $c_s = -0.2$ is very mild.

References

- [1] V. Silveira and A. Zee, Phys. Lett. B **161**, 136 (1985).
- [2] J. McDonald, Phys. Rev. D **50**, 3637 (1994) [arXiv:hep-ph/0702143].
- [3] C. P. Burgess, M. Pospelov and T. ter Veldhuis, Nucl. Phys. B **619**, 709 (2001) [arXiv:hep-ph/0011335].

- [4] H. Davoudiasl, R. Kitano, T. Li and H. Murayama, Phys. Lett. B **609**, 117 (2005) [arXiv:hep-ph/0405097].
- [5] L. Randall and R. Sundrum, Phys. Rev. Lett. **83**, 3370 (1999) [arXiv:hep-ph/9905221].
- [6] J. March-Russell, S. M. West, D. Cumberbatch and D. Hooper, JHEP **0807**, 058 (2008) [arXiv:0801.3440 [hep-ph]].
- [7] E. Komatsu *et al.* [WMAP Collaboration], arXiv:0803.0547 [astro-ph].
- [8] Z. Chacko, M. A. Luty and E. Pontón, JHEP **0007**, 036 (2000) [arXiv:hep-ph/9909248].
- [9] S. J. Huber and Q. Shafi, Phys. Lett. B **498**, 256 (2001) [arXiv:hep-ph/0010195]; S. J. Huber, Nucl. Phys. B **666**, 269 (2003) [arXiv:hep-ph/0303183].
- [10] K. Agashe, G. Perez and A. Soni, Phys. Rev. Lett. **93**, 201804 (2004) [arXiv:hep-ph/0406101]; K. Agashe, G. Perez and A. Soni, Phys. Rev. D **71**, 016002 (2005) [arXiv:hep-ph/0408134].
- [11] A. L. Fitzpatrick, G. Perez and L. Randall, arXiv:0710.1869 [hep-ph]; A. L. Fitzpatrick, L. Randall and G. Perez, Phys. Rev. Lett. **100**, 171604 (2008).
- [12] G. Perez and L. Randall, arXiv:0805.4652 [hep-ph].
- [13] H. Davoudiasl, J. L. Hewett and T. G. Rizzo, Phys. Rev. D **68**, 045002 (2003) [arXiv:hep-ph/0212279]. M. S. Carena, E. Pontón, T. M. P. Tait and C. E. M. Wagner, Phys. Rev. D **67**, 096006 (2003) [arXiv:hep-ph/0212307]. M. S. Carena, A. Delgado, E. Pontón, T. M. P. Tait and C. E. M. Wagner, Phys. Rev. D **71**, 015010 (2005) [arXiv:hep-ph/0410344].
- [14] L. Bergstrom, P. Ullio and J. H. Buckley, Astropart. Phys. **9**, 137 (1998) [arXiv:astro-ph/9712318].
- [15] B. Moore, T. R. Quinn, F. Governato, J. Stadel and G. Lake, Mon. Not. Roy. Astron. Soc. **310**, 1147 (1999) [arXiv:astro-ph/9903164].
- [16] J. F. Navarro, C. S. Frenk and S. D. M. White, Astrophys. J. **462**, 563 (1996) [arXiv:astro-ph/9508025].

- [17] B. Thomas, Phys. Rev. D **72**, 023519 (2005) [arXiv:hep-ph/0503248].
- [18] http://fermi.gsfc.nasa.gov/public/resources/pubs/factsheet/Sci_Fact_Sheet.pdf.
- [19] http://fermi.gsfc.nasa.gov/public/resources/pubs/gsd/GSD_web.pdf
- [20] G. D. Mack, T. D. Jacques, J. F. Beacom, N. F. Bell and H. Yuksel, Phys. Rev. D **78**, 063542 (2008) [arXiv:0803.0157 [astro-ph]].
- [21] L. Bergstrom and P. Ullio, Nucl. Phys. B **504**, 27 (1997) [arXiv:hep-ph/9706232].
- [22] Z. Bern, P. Gondolo and M. Perelstein, Phys. Lett. B **411**, 86 (1997) [arXiv:hep-ph/9706538].
- [23] K. Agashe, A. Delgado, M. J. May and R. Sundrum, JHEP **0308**, 050 (2003) [arXiv:hep-ph/0308036].
- [24] K. Agashe, R. Contino and A. Pomarol, Nucl. Phys. B **719**, 165 (2005) [arXiv:hep-ph/0412089].
- [25] K. Agashe, R. Contino, L. Da Rold and A. Pomarol, Phys. Lett. B **641**, 62 (2006) [arXiv:hep-ph/0605341].
- [26] M. S. Carena, E. Pontón, J. Santiago and C. E. M. Wagner, Nucl. Phys. B **759**, 202 (2006) [arXiv:hep-ph/0607106]; Phys. Rev. D **76**, 035006 (2007) [arXiv:hep-ph/0701055].
- [27] O. Adriani *et al.*, arXiv:0810.4995 [astro-ph].
- [28] J. Diemand, M. Kuhlen and P. Madau, Astrophys. J. **657**, 262 (2007) [arXiv:astro-ph/0611370].
- [29] I. V. Moskalenko and A. W. Strong, Phys. Rev. D **60**, 063003 (1999) [arXiv:astro-ph/9905283].
- [30] E. A. Baltz and J. Edsjo, Phys. Rev. D **59**, 023511 (1999) [arXiv:astro-ph/9808243].
- [31] S. W. Barwick *et al.* [HEAT Collaboration], Astrophys. J. **482** (1997) L191 [arXiv:astro-ph/9703192].

- [32] M. Aguilar *et al.* [AMS-01 Collaboration], *Phys. Lett. B* **646**, 145 (2007) [arXiv:astro-ph/0703154].
- [33] L. Bergstrom, T. Bringmann and J. Edsjo, arXiv:0808.3725 [astro-ph].
- [34] M. Cirelli and A. Strumia, arXiv:0808.3867 [astro-ph].
- [35] V. Barger, W. Y. Keung, D. Marfatia and G. Shaughnessy, arXiv:0809.0162 [hep-ph].
- [36] M. Cirelli, M. Kadastik, M. Raidal and A. Strumia, arXiv:0809.2409 [hep-ph].
- [37] N. Arkani-Hamed, D. P. Finkbeiner, T. Slatyer and N. Weiner, arXiv:0810.0713 [hep-ph].
- [38] J. Chang *et al.* [ATIC Collaboration], *Proc. of 29th International Cosmic Ray Conferences (ICRC 2005)*, Pune, India.
- [39] O. Adriani *et al.*, arXiv:0810.4994 [astro-ph].
- [40] T. Gherghetta and A. Pomarol, *Nucl. Phys. B* **586**, 141 (2000) [arXiv:hep-ph/0003129].